Available online at www.sciencedirect.com
SCIENCE DIRECT®
Journal of Catalysis 231 (2005) 453–467
JOURNAL OF CATALYSIS
www.elsevier.com/locate/jcat

Platinum tungstated zirconia isomerization catalysts Part I. Characterization of acid and metal properties

T.N. Vu [a], J. van Gestel [a,*], J.P. Gilson [a,b], C. Collet [b], J.P. Dath [b], J.C. Duchet [a]

[a] *Laboratoire Catalyse et Spectrochimie, CNRS-ENSICAEN, Université de Caen, 6, Bd. du Maréchal Juin, F-14050 Caen, France*
[b] *Total, ATOFINA Research S.A., Zone Industrielle C, B-7181 Feluy, Belgium*

Received 4 December 2004; revised 30 January 2005; accepted 31 January 2005

Available online 17 March 2005

Abstract

Tungstated zirconia catalysts containing 14–34 wt% W were prepared by bringing silica-modified hydrous zirconia into contact with appropriate amounts of metatungstate. The dry powders were extruded with an alumina binder and calcined at 1023 K. The extrudates were subsequently loaded with 0.1–1.5 wt% platinum and finally calcined at 753 K. The samples were characterized by means of XRD, nitrogen adsorption–desorption, and infrared spectroscopy. It is shown that silica stabilizes crystalline zirconia in the tetragonal phase and produces a high surface area and porous catalytic material. The presence of tungsten at coverages below the theoretical monolayer and the alumina binder hardly affects the structural and textural properties of such a silica-stabilized zirconia. Bulk tungsten oxide is detected for tungsten coverage exceeding the theoretical monolayer and induces the mechanical collapse of the alumina-bound extrudate. Low-temperature FT-IR spectra of adsorbed carbon monoxide gave the distributions of the Lewis and Brønsted acid sites. The tungstate species consume both Lewis and Brønsted sites of the zirconia up to the monolayer. A new Brønsted acidity of moderate strength is created at intermediate tungsten coverage. The concentration of these Brønsted sites, specific to the polytungstate species, increases with loading and reaches a maximum of one site for about three tungsten atoms at monolayer coverage. Beyond, this acidity decreases because of the coexistence of these polytungstates with bulk tungsten oxide. The high site density suggests the formation of a pseudo-heteropolyanion incorporating Zr^{4+} and most probably Si^{4+} ions, in line with a new infrared signal detected in the structure band region. The metallic function was characterized by the hydrogenation of toluene and CO adsorption. Both methods yield two linear domains with increasing platinum content, with a sharp increase around 0.2 wt% Pt. It is proposed that below this break point, the very low amount of accessible metal is due to the insertion of a large fraction of platinum into the zirconia subsurface. After saturation of the subsurface, additional platinum remains external and accessible. Correcting the platinum content for the imbedded species yields dispersion as high as 90% with a constant particle size of about 1 nm for accessible platinum in the whole range of concentration.

Keywords: Silica-stabilized tungstated zirconia; Alumina binder; Platinum; CO adsorption; IR characterization; Acidity; Acid sites distribution; Isomerization catalysts

1. Introduction

Since the pioneering works by Hino and Arata [1,2], tungstate- and sulfate-modified zirconias have become an important family of solid acid catalysts. A strong interest in their potential application in alkane isomerization is manifest. Commercial processes require their promotion with platinum to improve activity, stability, and selectivity in the presence of hydrogen [3–6]. Sulfated zirconias are more active than tungstated zirconias and therefore operate at lower temperatures, that is, under conditions more favorable (thermodynamically) for the production of branched isomers. However, they suffer from a poor stability due to a loss of sulfate by reduction or decomposition [7–9], under reaction or regeneration conditions. Tungsten oxide-based zirconias are more robust. To be active, they must be prepared from

* Corresponding author. Fax: (+33) 02 31 45 28 22.
E-mail address: jacob.vangestel@ensicaen.fr (J. van Gestel).

0021-9517/$ – see front matter
doi:10.1016/j.jcat.2005.01.037

amorphous zirconia and a tungsten compound, followed by calcination at high temperature to ensure zirconia crystallization. Intensive research over the past decade [10–21] has provided considerable insight into the bulk and surface structure of the tungstated zirconia catalysts. These studies showed that tungstate species stabilize crystalline zirconia in the tetragonal phase and prevent sintering. The nature of the WO_x species spread on the ZrO_2 surface, although still controversial, varies with tungsten loading. At low W content, they are present as tetrahedral [19,21] or distorted octahedral monomeric tungstate [3,22]. Oligomeric and polymeric species grow with increasing tungsten concentration [19,22]. They coexist with crystalline WO_3 oxide at high loading. The various domains are not well defined with respect to the W loading and depend on the preparation conditions and the temperature of calcination. The relation between the changes in surface structure upon loading and the theoretical monolayer is still controversial.

The nature of the tungstate species governs the acid properties of the solids. The loading with tungsten consumes the Lewis sites of zirconia, and new Brønsted acid sites are associated with the polytungstate clusters. However, the origin of the acidity is still under debate. According to the group of Iglesia, acidity is created during the reaction in the presence of hydrogen on quite large polytungstate species [13,14,23]. The arrangement of about 25 W atoms is required to delocalize the negative charge counterbalancing the protonic species. The group of Knözinger [11,12], on the other hand, highlights a permanent Brønsted acidity and proposes the formation of a pseudo-heteropolyanion by incorporation of Zr^{4+} ions into the polytungstate clusters. Although the results were rather conclusive for catalysts loaded at intermediate tungsten coverage, the results for acid titration with basic compounds or hydrogen did not allow correlation of acidity with activity in the whole range of tungsten densities [14,23,24].

Our aim is to study tungstated zirconia catalysts to quantify and relate acidity with their activity in *n*-hexane isomerization under industrially relevant conditions. To this end, the catalysts were shaped as extrudates with an alumina binder and loaded with platinum. Moreover, we used a silica-stabilized zirconia because the crystallinity and the surface area of the zirconia carrier are known to be strongly influenced by the tungsten loading and the temperature of calcination [11–15,17,18]. The effect of tungsten on the creation of acid sites should be more clearly indicated on a structurally and texturally stable zirconia.

We report in Part I the physicochemical characterization of such $Pt/WO_3–ZrO_2$ isomerization catalysts. We first focus on the influence of the alumina binder on the structure, texture, and surface properties of the silica-zirconia carrier. Then we examine the tungstated zirconia samples containing between 14 and 34 wt% W, with a special emphasis on acid site speciation and quantification by low-temperature FT-IR spectroscopy of adsorbed carbon monoxide. Finally, we characterize platinum accessibility by toluene hydrogenation and CO adsorption.

These characterizations will be used in Part II to better understand the effect of tungsten and platinum loadings on the mechanism of isomerization of *n*-hexane.

2. Experimental

2.1. Catalysts

We used a silica-doped zirconia (3 wt% SiO_2) to obtain the tungstated zirconia catalysts. It was prepared as follows [25]: zirconium hydroxide was precipitated from an aqueous solution of zirconyl nitrate with ammonium hydroxide. We introduced silicon into the gel by adding an aqueous solution of Ludox AS-40 colloidal silica. The $ZrO_2–SiO_2$ gel was then washed and dried at 393 K overnight to obtain a zirconia powder. The solid material was then immersed in an aqueous solution (liquid/solid ratio 6 ml g^{-1}) of ammonium metatungstate (14–34 wt% W in the $ZrO_2–SiO_2–WO_x$ mixture) in a rotavapor apparatus and outgassed under vacuum, and the excess liquid was evaporated at about 60 °C. After drying, the powder was mixed with Condea Pural SB xerogel alumina (20 wt% alumina) and wetted to make extrusion possible. The extrudates (5 × 1.6 mm) were subsequently dried and calcined at 1023 K for 3 h in air flow (heating rate 2 K min^{-1}). A tungsten-free zirconia sample was prepared in the same way. The final extrudates of tungstated zirconia are labeled *x*W/SiZ-Al, where *x* represents the W content (wt%) on the *x*W/SiZ basis. The extension -Al is added to indicate whether extrudates were used. For instance, SiZ and SiZ-Al represent unshaped and alumina-bound silica-doped zirconia, respectively. Platinum ($y = 0.1–1.5$ wt%) was deposited on the W/SiZ-Al extrudates by pore volume impregnation with an aqueous solution of H_2PtCl_6, followed by calcination in air at 753 K for 3 h (heating rate 2 K min^{-1}). The final catalysts are thus abbreviated *y*Pt/*x*W/SiZ-Al.

2.2. XRD characterization

Powder X-ray diffraction patterns were recorded on a Philips PW1750 spectrometer with Cu-K_α radiation. Each step of 0.02° was measured for 5 s from 5° to 70° (2θ).

2.3. FT-IR characterization

The acid and metallic properties of the Pt/W/SiZ-Al catalysts were characterized by FT-IR spectroscopy with CO as a probe molecule. Infrared spectra were recorded with a Nicolet Magma 550 spectrometer equipped with a MCT detector. The extrudates were crushed and the resulting powder was pressed into self-supported wafers (∼ 20 mg). Activation was carried out in situ in a flow IR cell under dry air at 673 K for 2 h (heating rate 3 K min^{-1}). Air was then

replaced by dry and oxygen-free nitrogen, and the temperature was brought down to 523 K for 1 h. The sample was then treated under purified hydrogen at 523 K for 1 h and finally evacuated at room temperature for 1 h before FT-IR characterizations. The activation procedure, with the notable exception of pressure, was identical to the one used in the catalytic test (Part II of this article). CO was first adsorbed on the sample at room temperature to characterize the metallic function of the catalyst. The wafer was then evacuated at 473 K for 1 h and cooled to 100 K for the characterization of Lewis and Brønsted acid sites by CO adsorption. Spectra were recorded at room temperature (metallic function characterization) or at 100 K (acid function characterization).

2.4. Hydrogenation of toluene

Hydrogenation of toluene (0.026 bar of toluene) was carried at 423 or 523 K in a dynamic glass reactor operating at atmospheric pressure, with a flow of 90 ml min^{-1} of the toluene–hydrogen mixture. Reaction products were analyzed on-line with a Varian 3900 gas chromatograph equipped with a 50 m Chrompack CP-SIL 5B column and a FID detector. The reaction rate was determined under varying conditions (toluene conversion $< 7\%$ by adjustment of the mass of catalyst). Before the catalytic test, the catalyst was activated in flowing air and reduced in hydrogen flow according to the same procedure as for IR characterization.

Toluene (Carlo ERBA, 99.5%) and air (Air Liquide, grade I) were dried over an activated 3A zeolite. Hydrogen and nitrogen (Air Liquide, grade I) were further purified from water and oxygen contaminants by 3A zeolite and BTS (Fluka) traps.

2.5. Other characterizations

Specific surface areas and pore size distributions of the catalysts were determined from nitrogen adsorption–desorption isotherms measured on an ASAP 2000 (Micromeritics) after outgassing at 573 K in dynamic vacuum for 1 h. The data were processed with the BET and BJH methods.

Elementary analysis of the samples was performed at the Service Central d'Analyse (CNRS Vernaison).

3. Results and discussion

3.1. Characterization of the Si-zirconia carrier: effect of binding with alumina

The zirconia used for our tungstated catalysts was doped with silica to stabilize its structure and maintain a high surface area [25]. Various cations can be accommodated by zirconia, to stabilize its tetragonal form and prevent sintering at high temperature [26]. Such a silica-zirconia carrier differs from those generally described in the open literature; it is therefore important to first characterize the structure and the surface properties of these preparations. Moreover, we report in Part II a kinetic study of the isomerization of *n*-hexane on the very same catalysts. The activity data have been measured on platinum tungstated zirconia catalysts shaped as extrudates with an alumina binder. The effect of the alumina binder on the physicochemical properties of the silica-zirconia must also be assessed.

3.1.1. Structural and textural properties

XRD patterns (Fig. 1) show the crystalline structure of the silica-zirconia for the unshaped (SiZ) and extrudate (SiZ-Al) samples after calcination at 1023 K.

Both solids exhibit mainly the tetragonal phase of zirconia, a small amount of the cubic form (line at 63°), and no trace of the monoclinic phase. Silica has an effect similar to that of the other stabilizing agents (Ca, Y), that is, it retards the phase transformation into the thermodynamically more stable monoclinic form upon high-temperature calcination [27]. The crystallite size determined from the Scherrer equation (line at $2\theta \cong 50°$) was found to be as small as 5.7 nm and highlights the high degree of stabilization brought about by silica incorporation into the zirconia matrix. The XRD pattern of the extrudates does not yield any evidence of a crystalline phase of the alumina binder. The structural features of the zirconia, crystal phases, and crystal size remain unchanged upon shaping, as was the case for sulfated zirconia [28]. This suggests a simple dilution effect of the alumina in the extrudates, in contrast to the deep structural changes reported for coprecipitated alumina and zirconia mixed oxides [29,30] or sulfated zirconia supported on alumina [31].

The textural properties of such silica-stabilized zirconia are interesting for catalysis, since the BET surface area of the unshaped material, calcined at 1023 K, reaches 176 $m^2\,g^{-1}$ and the pore volume reaches 0.31 $cm^3\,g^{-1}$ (Table 1). The nitrogen adsorption–desorption isotherms in Fig. 2 are of type IV and display a type E hysteresis. This is indicative of mesopores created by packing of spheroid particles.

The pore size distribution calculated from the desorption branch is monomodal and is centered at 7-nm diameter. The cumulative surface closely matches the BET area and confirms the absence of micropores. It compares well with the geometrical area ($S_{geo} = 173\ m^2\,g^{-1}$, Table 1) calculated from the crystallite size of zirconia, under the assumption of cubic crystals.

Binding with alumina does not significantly affect the shape of the isotherms. However, the BET surface area is increased by 10% and the pore volume by 16% (Table 1). The mean pore diameter is not affected, and the accessibility to the zirconia surface remains high.

These changes in textural properties without modification of the zirconia structure agree with a physical effect of the binder. In contrast to the examples reported in the literature, our procedure does not favor alumina incorporation into the zirconia structure. Indeed, wetting is kept at a minimum dur-

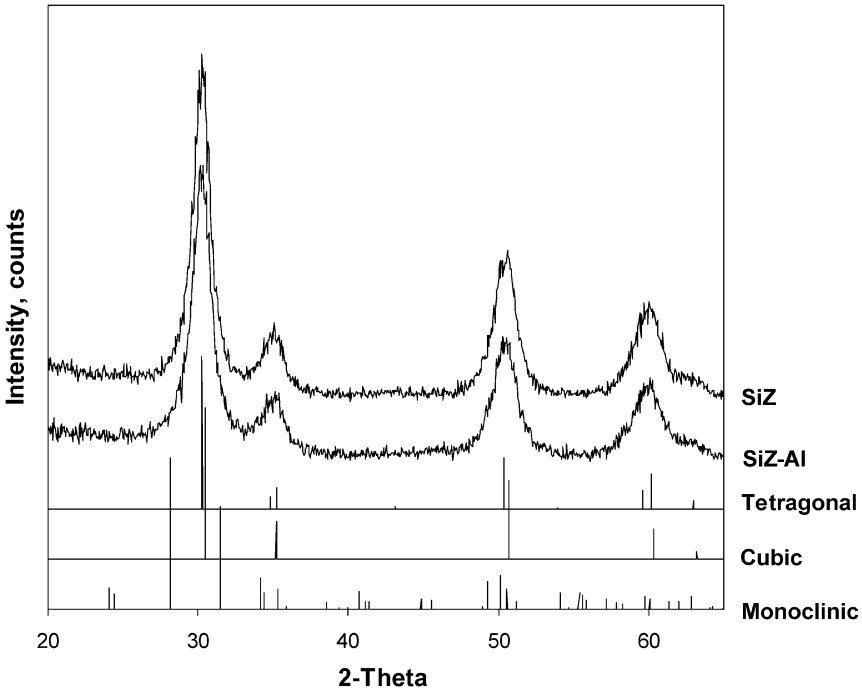

Fig. 1. Powder X-ray diffraction patterns of zirconia (SiZ) and alumina-bound (SiZ-Al) zirconia. Reference patterns were taken from the JCPDS files: 88-1007 (tetragonal); 27-0997 (cubic) and 88-2390 (monoclinic).

Table 1
Composition and physico-chemical properties of the tungstated zirconia samples

Sample	W (wt% g^{-1} W/SiZ)	S_{BET} (m^2 g^{-1})	Pore volume (cm^3 g^{-1})	d crystal[a] (nm)	S_{geo}[b] (m^2 g^{-1} WSiZ)	W density (at nm^{-2} ZrO_2)
SiZ	0.0	176	0.31	5.7	173	0.0
SiZ-Al	0.0	195	0.36	5.7	173	0.0
14W/SiZ-Al	14.3	158	0.33	5.7	141	3.2
16W/SiZ-Al	16.0	156	0.35	5.8	136	3.9
22W/SiZ-Al	21.8	146	0.31	5.7	125	5.8
27W/SiZ-Al	27.4	126	0.32	5.8	111	8.1
34W/SiZ-Al	34.0	109	0.31	5.7	98	11.4

[a] Crystallite size from XRD lines at ∼50° (2θ).
[b] Geometrical area calculated from crystallite size of zirconia.

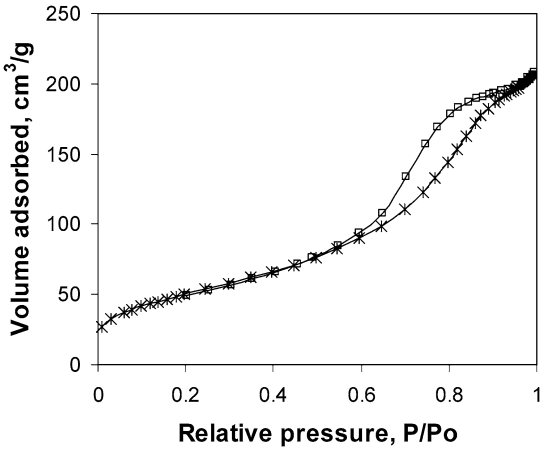

Fig. 2. Nitrogen adsorption–desorption isotherms of the unshaped SiZ zirconia.

ing the preparation of the extrusion paste, in contrast to the co-precipitation of the hydroxides or prolonged mixing of the two hydroxides in excess water [29,30].

3.1.2. Infrared characterization of the silica-zirconia carrier

The surface properties of the SiZ and SiZ-Al zirconia carriers were measured by infrared spectroscopy. After activation under hydrogen in the flow cell, the catalyst wafer was evacuated at 473 K for 1 h to eliminate traces of water, if any. This step is absolutely mandatory for the measurement of acidity on a material as close to the catalyst tested in Part II.

Fig. 3 presents room-temperature infrared spectra for the OH stretching region for both alumina-bound (SiZ-Al) and unshaped (SiZ) zirconias. The main band at 3743 cm^{-1} in the spectra of the zirconia indicates a high concentration

of silanol groups, resulting from our preparation method. The presence of silica strongly modifies the overall profile of the hydroxyl groups for pure zirconia: there is no evidence for terminal OH groups (∼3760 cm^{-1}) characteristic of tetragonal zirconia, although this band is not expected to be intense on stabilized tetragonal zirconia [27,32]. The less basic hydroxyl groups are present at ∼3675 cm^{-1}. This band is usually attributed to bridged OH groups, and its frequency strongly depends on the hydration degree of the sample [32]. Shaping with alumina consumes part of both silanol and Zr-bridged OH groups, as indicated by the difference spectra. No signal for well-defined Al–OH groups at about 3560 cm^{-1} is observed. These results point to some interaction of the alumina binder with the surface of the stabilized zirconia. However, the influence of the binder is minor compared with the drastic changes in the OH region on co-precipitated zirconia and alumina preparations [30]. Again, this is evidence that such an extrusion minimizes the impact of alumina on zirconia.

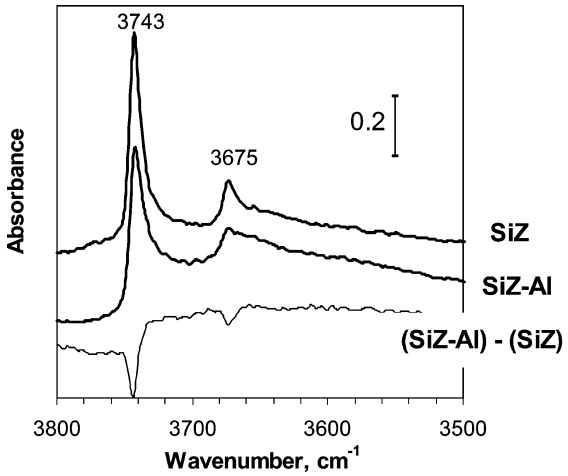

Fig. 3. FT-IR spectra of alumina-bound zirconia (SiZ-Al), zirconia (SiZ), and the difference between them in the hydroxyl region. Spectra were normalized for the same mass of zirconia.

The acid properties of the carrier were checked by the IR signal of CO adsorbed at low temperature. Figs. 4A and 4B gather the spectra (CO stretching region) recorded on alumina free (SiZ) and extruded (SiZ-Al) zirconias after adsorption of incremental doses of the CO probe molecule. Three types of CO interacting with the surface are observed at ca. 2190, 2160, and 2143 cm^{-1}. They are characteristic of coordination to cationic sites and hydrogen-bonded and physisorbed CO, respectively, in agreement with the literature [12,26].

On the SiZ sample of zirconia (Fig. 4A), the very first carbonyl band is recorded at 2188 cm^{-1}, and a second signal readily appears at 2179 cm^{-1} with increasing CO concentration. They are assigned to CO bonding to Zr^{4+} centers acting as weak Lewis acid sites. Similar distinct Lewis sites were reported by Scheithauer et al. [11] and Morterra et al. [33] and associated with different defects of the crystalline zirconia. The two bands become unresolved at 2180 cm^{-1} for higher CO concentration, and the growing signal at 2165 cm^{-1} indicates the interaction of CO with Brønsted sites. The H-bonded CO band shifts to lower wave numbers as the CO concentration is increased. Simultaneously, the signal in the OH region (not shown) is shifted to lower wave numbers by perturbation by adsorbed CO. Compared with the original spectrum before CO adsorption in Fig. 3, the band around 3675 cm^{-1} progressively disappears and a broad signal grows from 3500 cm^{-1} for low CO concentration to 3530 cm^{-1} for higher CO concentration; it is indicative of H-bonding with acidic OH groups of the zirconia. For the highest CO doses, the silanol band at 3743 cm^{-1} is also shifted to 3640 cm^{-1}. Although relatively inaccurate, the frequency shift $\Delta\nu_{OH}$ and the frequency of CO adsorbed may be used to estimate the relative strengths of the OH groups [34]. For our zirconia, $\Delta\nu_{OH}$ were ca. 175–145 cm^{-1} and ν_{CO} changed from 2166 to 2157 cm^{-1}, corresponding to a moderate Brønsted acidity.

Similar data are displayed on Fig. 4B for the alumina-bound SiZ-Al zirconia. The bands are broader than for the

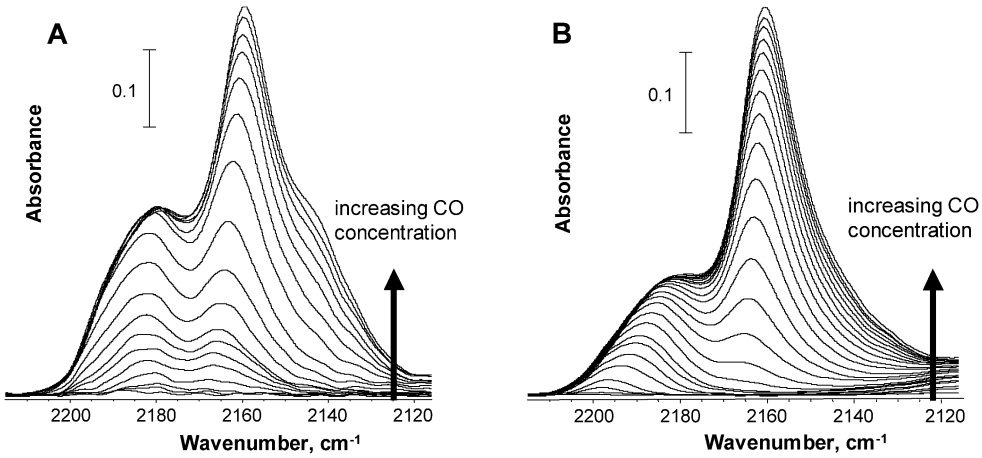

Fig. 4. FT-IR spectra of adsorbed CO at 100 K on (A): unshaped SiZ zirconia, and (B): alumina-bound SiZ-Al zirconia. CO concentration was increased from 0 to 750 µmol CO g^{-1} (A) and from 0 to 1000 µmol CO g^{-1} (B).

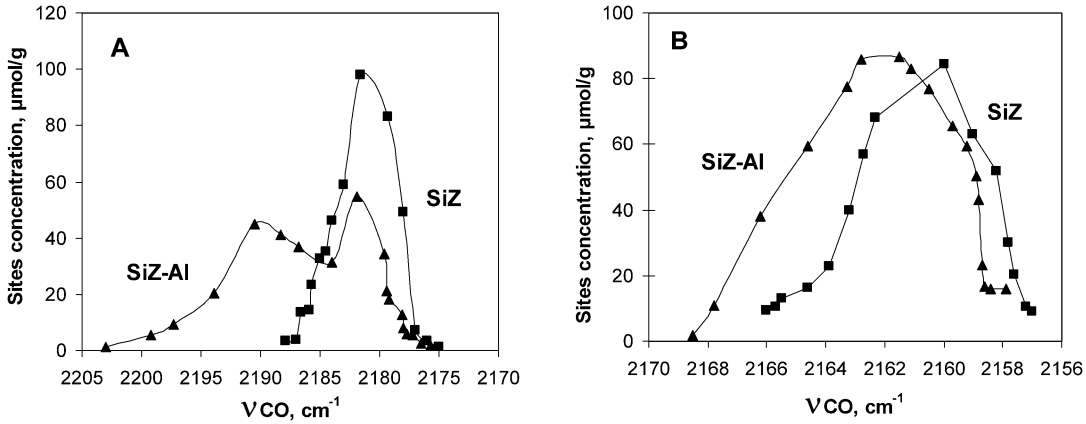

Fig. 5. Distributions of acid sites on zirconia (SiZ) and alumina-bound zirconia (SiZ-Al). (A) Lewis; (B) Brønsted.

unshaped zirconia. The Lewis sites region gives a single signal at 2198 cm^{-1}, shifting to 2175 cm^{-1} with increasing CO concentration. Therefore, the distribution of acid sites is broader than on the alumina-free zirconia sites. Moreover, the higher frequency of carbonyl stretching in this region seems to reflect a stronger Lewis acidity than on the alumina-free zirconia. This is also the case for the Brønsted acid sites, since the corresponding band is recorded at 2168 cm^{-1}, again shifted downward to 2158 cm^{-1} with increasing CO concentration. Apparently, the presence of alumina has slightly reinforced the acid properties of the zirconia carrier.

A more complete analysis of the data makes it possible to plot the distribution of the Lewis and Brønsted acid strength, that is, the number of sites versus their wave number. This distribution is inferred from the variation in the corresponding infrared bands in both position and intensity between two successive CO concentrations. Between two successive CO doses, additional sites are detected. Their strength is characterized by the wave number of the IR band in difference spectra. Their number is evaluated from the area of this IR band with the use of the extinction coefficients for the CO bands for Lewis and Brønsted acid sites. These molar extinction coefficients (ε) were determined, as usual, from the variation of the band intensity with the amount of CO adsorbed on Lewis and Brønsted sites. We found $\varepsilon_L = 2.5\ \mu mol^{-1}\ cm^{-1}$ and $\varepsilon_B = 1.5\ \mu mol^{-1}\ cm^{-1}$ for Lewis and Brønsted sites, respectively.

Figs. 5A and 5B compare the distributions of Lewis and Brønsted sites on the unshaped and extruded zirconia samples. These distributions are more informative than the spectra for tracking the influence of the alumina binder on acidity. The global distribution of Lewis sites (Fig. 5A) has changed from monomodal to bimodal upon alumina extrusion. The first maximum at ca. 2191 cm^{-1} closely corresponds to the Lewis sites that are observed on pure alumina [35]. The second maximum at 2182 cm^{-1} represents the original Lewis sites of the zirconia itself, but about half of the sites have disappeared. Some alumina must have interacted with the zirconia defects, as already observed in the OH region. The distribution relative to the Brønsted acid sites (Fig. 5B) is centered around 2160 cm^{-1} on the SiZ zirconia and at 2162 cm^{-1} in the presence of alumina (SiZ-Al). This difference is hardly significant. The signal for pure alumina, expected at 2155 cm^{-1} [36], is not observed, in agreement with the absence of the corresponding OH signal. However, the Brønsted distribution becomes broader with a higher wave number.

To conclude, the effect of alumina on the acid properties of the silica-zirconia carrier is very limited and indicative of mainly a dilution effect.

3.2. Tungstated zirconia: effect of tungsten loading on structure and texture

On tungstated zirconia catalysts, an important parameter is the tungsten density. Indeed, the literature [3,19,22] reports changes in the nature of the supported tungsten species with loading. Since the polymeric species are proposed to be responsible for the catalytic activity in a number of reactions, especially isomerization, it is of prime importance to determine the tungsten content for which their formation is at maximum, that is, at monolayer coverage. We first examined the XRD patterns of our series of samples, loaded with tungsten concentrations ranging from 14 to 34 wt% W, expressed on the xW/SiZ basis. The composition of the samples is reported in Table 1.

3.2.1. XRD characterization

The XRD patterns of the tungstated zirconia extrudates calcined at 1023 K are presented in Fig. 6. All of the xW/SiZ-Al samples of the series show crystalline phases similar to those of the zirconia and the SiZ-Al carrier, namely tetragonal with a small cubic contribution. This result contrasts with those reported in the literature for which the tungsten content has a strong effect on the fraction of tetragonal phase [13,18,37–39]. Indeed, the authors show that the first load of WO_x species stabilizes the zirconia structure and prevents sintering of the tetragonal crystallites. In our case, the tungsten loading does not change the XRD

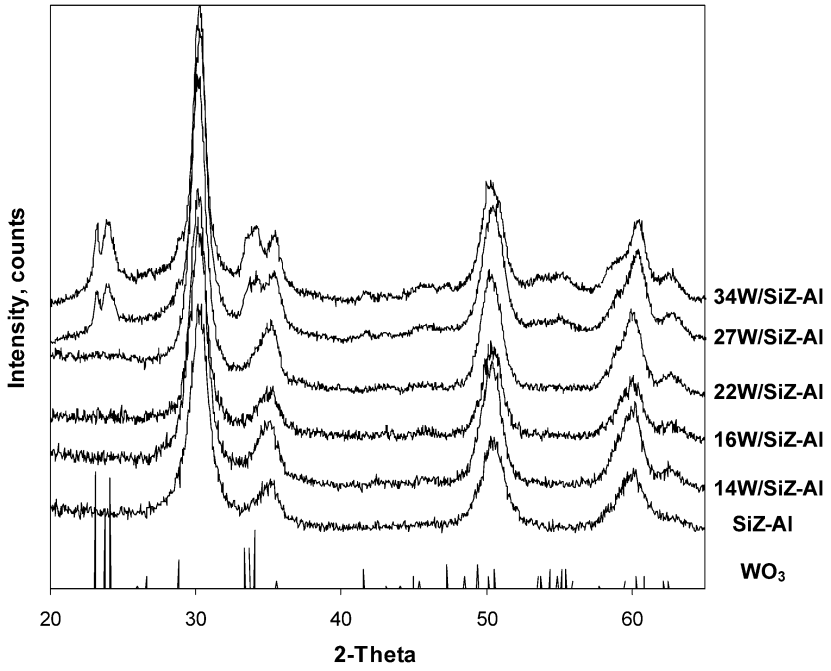

Fig. 6. X-ray diffraction patterns of SiZ-Al and *x*W/SiZ-Al extrudate samples. Reference pattern of orthorhombic WO_3 oxide was taken from the JCPDS file 20-1324.

pattern of the zirconia carrier, since the stabilization of the structure is already achieved by incorporation of silicon in the preparation [25]. However, the appearance of the line at 63° (2θ) with tungsten loading may reflect a small increase in the cubic phase.

The mean particle size of the zirconia crystallites, estimated from the Scherrer equation (the reflection at $2\theta \cong 50°$), was found to be almost constant, independently of the tungsten content (Table 1). It is the same value as for the bare carrier. Our preparation yields particles as small as 5.7 nm, smaller by a factor of 3 than those reported by others [11,13,18]. Again, this can be attributed to the stabilizing effect of silica. Bulk tungsten oxide, identified as orthorhombic WO_3, appears on the catalysts loaded with 27 and 34 wt% tungsten. This was expected from the yellow color of the samples. Apparently, lower contents yield uniformly spread oxotungsten species, indicating that the full capacity of the zirconia carrier (monolayer coverage) has been reached for 22 wt% tungsten.

3.2.2. Surface area

The numerous data reported in the literature [4,11–15,17,18,37] point to large variations in the surface area of crystallized tungstated zirconia with the calcination temperature and with tungsten loading. In a homogeneous series of samples (i.e., calcined at the same temperature), the surface area goes through a maximum with tungsten concentration. It shifts to lower tungsten content as the temperature increases. For instance, in the study reported by Scheithauer et al. [11], the maximum shifts from ∼18 to ∼10 wt% WO_3 between 923 K and 1098 K. However, if the loading is expressed as tungsten density, that is, as W atoms per nm^2 ZrO_2, the position of the maximum is almost identical, ∼5 to 6 W nm^{-2}. The same value is found in other studies on tungstated zirconia [12,15,37]. It is very close to the theoretical monolayer calculated from the molecular area occupied by a WO_3 unit in bulk trioxide. We may conclude that tungsten species stabilize the crystalline structure of zirconia up to the monolayer coverage. Indeed, beyond the maximum, the surface area per gram of zirconia remains almost constant for samples loaded with as much as twice the monolayer coverage.

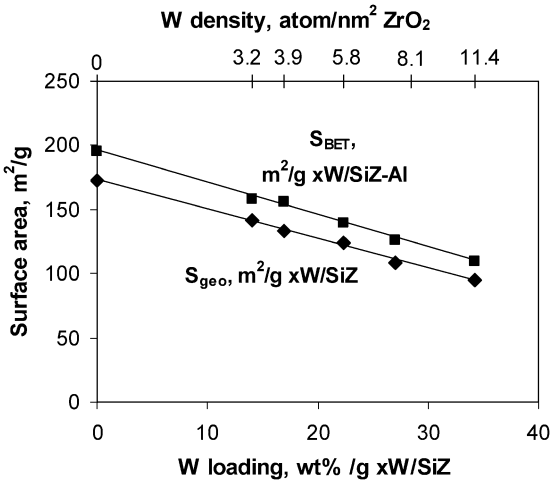

Fig. 7. BET surface area (S_{BET}) and geometrical area (S_{geo}) estimated from XRD as a function of tungsten loading or tungsten density in the *x*W/SiZ-Al extrudate samples.

Our samples of tungstated zirconia do not display the same behavior. The BET surface area of our W/SiZ-Al samples extruded with 20 wt% alumina (Table 1 and Fig. 7) decreases regularly with tungsten concentration, without any

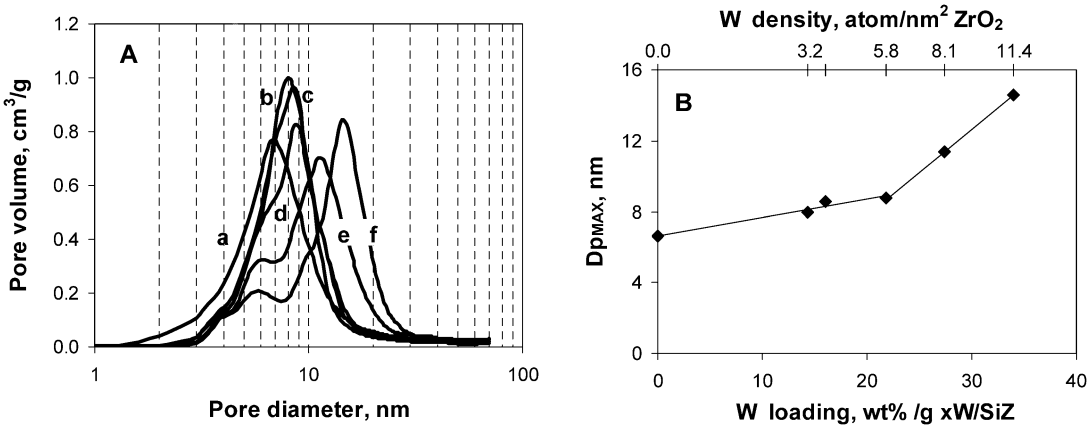

Fig. 8. (A) Pore size distribution of the SiZ-Al and xW/SiZ-Al extrudate samples: (a) SiZ-Al, (b) 14W/SiZ-Al, (c) 16W/SiZ-Al, (d) 22W/SiZ-Al, (e) 27W/SiZ-Al, (f) 34W/SiZ-Al. (B) Effect of tungsten loading on maximum pore diameter of alumina-bound zirconia SiZ-Al and xW/SiZ-Al extrudate samples.

maximum. Since our catalysts are shaped with an alumina binder, the BET surface area of the extrudates differs from that of the tungstated zirconia itself. Although the tungsten density is not directly accessible from the BET measurements, we need the surface of the zirconia carrier in the tungstated catalysts. It can simply be determined from the XRD data by application of the Scherrer formula. We can then calculate the geometrical area of the zirconia, assuming cubic crystals. Values gathered in Table 1 indicate a constant size at ∼6 nm, independently of the tungsten content corresponding to a geometrical area of 173 $m^2\,g^{-1}$ of zirconia, in agreement with the BET measurement (176 $m^2\,g^{-1}$) for the tungsten- and binder-free zirconia SiZ. The geometrical area of the W/SiZ component (without alumina) of the samples was calculated by weight correction for tungsten content. The plot in Fig. 7 shows a linear decrease in the geometrical area per gram of W/SiZ with tungsten content, which parallels the BET area of the extrudates. The difference represents an excess BET surface area brought about by the 20 wt% alumina binder corresponding to about 15 $m^2\,g^{-1}$ of the final samples. With respect to the tungsten density, the linear decrease in geometrical area follows that observed with the loading, without any singularity at the monolayer coverage, due to the constant surface area of the silica-zirconia carrier. In that sense, our series of samples of silica-stabilized zirconia appears to be very homogeneous (constant particle size) and makes it possible to investigate more easily the sole effect of tungsten loading on the physicochemical properties of the supported tungstate phase.

3.2.3. Pore size distribution

Fig. 8A presents the distributions in pore diameter of the series of tungstated zirconia extrudates. The main feature is a marked increase in pore diameter for the samples that were highly loaded (i.e. 27 and 34 wt% W), which show a bimodal distribution. A lower tungsten content (14 to 22 wt% W) yields a pore diameter distribution centered between 8 and 9 nm, almost independently of the loading. These changes are best visualized in Fig. 8B, where the pore diameter at maximum of the distribution ($D_{p_{max}}$) is plotted against tungsten loading or tungsten density. Opening of the pores occurs suddenly above 22 wt% W, indicated by the appearance of a second contribution at higher pore diameter. Interestingly, this change corresponds to the lower concentration limit, where bulk tungsten oxide is detected by XRD. It also marks the limit of the full monolayer coverage of the silica-zirconia carrier by tungstate species, ∼6 W nm^{-2}. Such a behavior is intriguing. For comparison, we measured the 27W/SiZ and 34W/SiZ samples without the alumina binder. Their pore size distribution reasonably compares with those of low loaded samples and does not present opening of the texture. The key feature of the phenomenon is the formation of bulk tungsten trioxide in the presence of the alumina binder. Presumably, the growth of WO_3 provokes cracks within the alumina layer and expands the texture. It is worth noting the poor mechanical properties of the 27W/SiZ-Al and 34W/SiZ-Al samples, thus confirming that the alumina no longer acts as a binding agent. In our tungstated zirconia catalysts, the presence of binder therefore allows a new and simple determination of the tungstate monolayer.

3.3. Tungstated zirconia: infrared characterization at room temperature

3.3.1. Hydroxyl stretching region

The OH stretching region of the room-temperature infrared spectra of the W/SiZ-Al extruded catalysts is shown in Fig. 9.

Compared with the (W free) SiZ-Al extrudate, the intensity of the overall spectra strongly diminishes with the introduction of 14 wt% tungsten (∼3 W atoms nm^{-2} ZrO_2). Both ZrOH and SiOH bands have been partially consumed. The ZrOH band at 3675 cm^{-1} has changed to a very broad signal shifted slightly to a lower wave number, whereas the SiOH hydroxyl band remains at the same position. Further loading has much less effect up to 22 wt% W, but both OH signals have totally disappeared for the catalysts containing

27 and 34 wt% W, that is, for coverage of the surface exceeding the monolayer. The absence of residual OH groups of zirconia at saturation coverage by tungsten was observed by others [12] and interpreted as a preferential formation of Zr–O–W terminations of the crystallite planes rather than OH groups. This is consistent with the anchoring of tungstate species on the carrier.

3.3.2. Structure band region

The spectra in the 950–1300 cm^{-1} domain (Fig. 10A) also indicate changes in the surface structure with tungsten loading. The Si-stabilized zirconia SiZ-Al itself (spectrum a) exhibits a broad band centered around 1020 cm^{-1}.

On the 14 wt% tungsten (spectrum b) sample, a new well-defined signal emerges at 1019 cm^{-1} with a shoulder at 1010 cm^{-1}. These are the typical W=O stretching bands described in the literature [11] as two independent surface oxo-species. With increased tungsten loading, the position of the main band is unchanged, but its intensity increases up to 22 wt% W (spectrum c), then levels off. Such an evolution remarkably follows the buildup of the monolayer. For the highest tungsten concentrations, we cannot find new IR bands at 750 cm^{-1} [20] for the bulk tungsten oxide identified by XRD, because of the strong absorbance of the alumina binder.

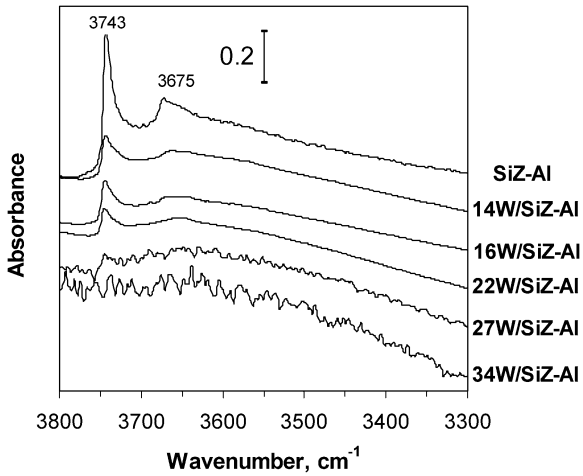

Fig. 9. FT-IR spectra in the hydroxyl region of the xW/SiZ-Al extrudate samples.

The presence of tungsten creates also a wide band at $\sim$1060 cm^{-1} for 14 wt% W. Such a signal has not been described for tungstated zirconia [12,20,40], so it must be specific to our preparation. Indeed, it does not appear on silica-free zirconia and is not influenced by the alumina binder. We postulate that the signal bears the fingerprint of the interaction between W atoms and the Si–O–Zr surface structure. However, because of the important variation in absorbance of the bare silica-zirconia in this region, difference spectra between the W/SiZ-Al samples and the SiZ-Al carrier (Fig. 10B) are more appropriate than the direct spectra in an appraisal of these changes.

They reveal the creation of a wide and flat signal between ca. 1050 and 1250 cm^{-1}. Most important is the change in intensity with tungsten content: it rapidly increases to 22 wt% W and suddenly decreases at 27 wt% W without an important further change at 34 wt% W. Again, the break point at 22 wt% W remarkably reflects the full monolayer coverage. Note that the two samples with the highest loading yield almost equivalent profiles while they contain increasing concentrations of bulk WO_3.

3.4. Tungstated zirconia: acid sites characterization by infrared spectroscopy of adsorbed carbon monoxide at low temperature

3.4.1. Low-temperature adsorption spectra

Adsorption of CO at liquid nitrogen temperature is well known to characterize both Lewis and Brønsted acid sites on a solid surface. We first describe results obtained on the 14W/SiZ-Al sample, loaded below the monolayer coverage in tungsten.

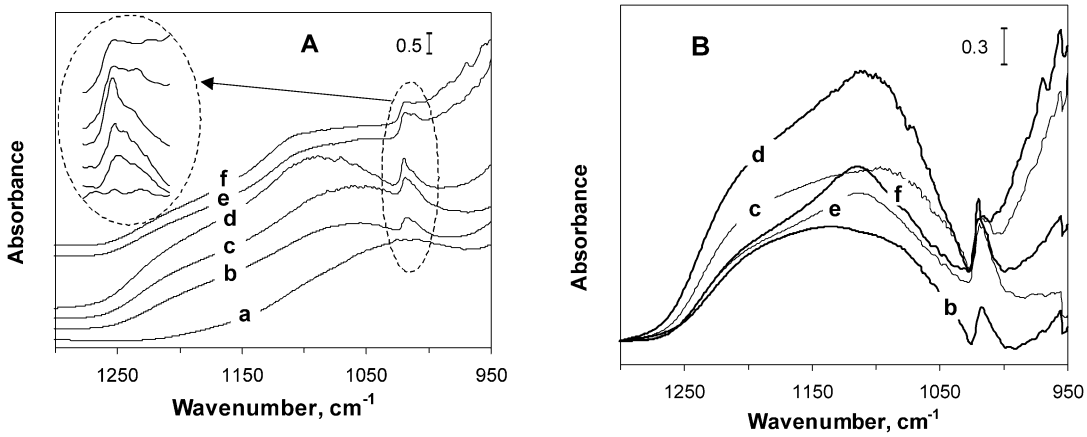

Fig. 10. (A) FT-IR spectra in the structure region of the alumina-bound SiZ-Al zirconia and xW/SiZ-Al extrudate samples: (a) SiZ-Al, (b) 14W/SiZ-Al, (c) 16W/SiZ-Al, (d) 22W/SiZ-Al, (e) 27W/SiZ-Al, (f) 34W/SiZ-Al. In the inset: W=O region. (B) Difference between xW/SiZ-Al and SiZ-Al spectra. Spectra were normalized for the same mass of zirconia.

Fig. 11 displays the CO stretching region of the spectra recorded upon introduction of incremental doses of the probe molecule. Comparing with the spectra of the alumina-bound zirconia (Fig. 4B), the presence of 14 wt% W reveals a red shift of the CO frequency bands on the carrier. The Lewis acid sites are now detected between 2200 and 2180 cm^{-1}. They require less CO to be saturated. There is no evidence for CO bonding on W^{6+} species, known to appear at higher wave number, ~2215 cm^{-1} [17]. The CO interacting with Brønsted sites appears at 2173 cm^{-1} and shifts down to 2158 cm^{-1} with increasing CO concentration. The introduction of tungsten on zirconia enhances both Lewis and Brønsted acid strength, in agreement with the observations of others [12,17].

The changes in acidity brought about by 14 wt% tungsten are more clearly indicated by the distribution of sites presented in Figs. 12A and 12B. They were obtained according to the method developed for the bare carrier and described before. It is then clear that the apparent enhanced Lewis acidity is in fact the result of the change from a bimodal to a monomodal distribution. A large fraction of the weak coordination centers of the zirconia component (L_{Zr}, 2182 cm^{-1}) has decreased with the introduction of 14 wt% tungsten, whereas the contribution of the alumina to the Lewis acidity (L_{Al}, 2191 cm^{-1}) has hardly been modified. Consequently, the entire IR carbonyl stretching bands (Fig. 11) appear at higher wave number upon tungsten loading. We conclude that tungstate species do not enhance or create Lewis acidity, but just consume the Lewis sites of the zirconia carrier. The distribution of the Brønsted acid sites (Fig. 12B) is shifted to and broadened on the high wave number side. A stronger acidity has thus been generated by the tungsten species. Nevertheless, since the loading with 14 wt% W does not cover the whole surface, the distribution includes some Brønsted sites specific to the zirconia carrier. Indeed, this distribution was very satisfactorily modeled by the sum of two gaussian distributions centered at 2162 and 2167 cm^{-1}. Since the former band corresponds to the signal for zirconia (B_{Zr}), the latter must be attributed to new stronger acid sites associated with the tungstate species (B_W).

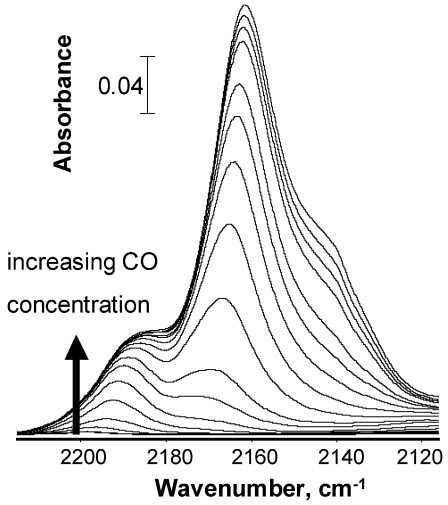

Fig. 11. FT-IR spectra of adsorbed CO at 100 K on the 14W/SiZ-Al extrudate. CO concentration was increased from 0 to 750 µmol CO g^{-1}.

This conclusion is confirmed by the changes in acid site distributions that occur with increasing tungsten concentration. The Lewis and Brønsted distributions obtained for the series of tungstated zirconia catalysts are collected in Figs. 13A and 13B. The number of Lewis acid sites on the 34W/SiZ-Al is too low to obtain an accurate distribution and is therefore not shown.

The influence of tungsten loading on Lewis acidity (Fig. 13A) can be summarized as follows: (i) the Lewis sites belonging to zirconia (~2182 cm^{-1}) progressively vanish up to the monolayer coverage (22 wt% W); (ii) the coordination of CO on the alumina component (~2191 cm^{-1}) becomes slightly stronger, suggesting an interaction of tungstate species with the binder, especially as the concentration exceeds the monolayer. Therefore, tungsten species first saturate the zirconia surface, and the excess migrates to the alumina, as shown by the important decrease in site concentration. This is in agreement with the conclusion drawn from the textural properties of the W/SiZ series. With respect to the Brønsted acid sites (Fig. 13B), the distribution is shifted from 2162 to 2167 cm^{-1} and narrows when

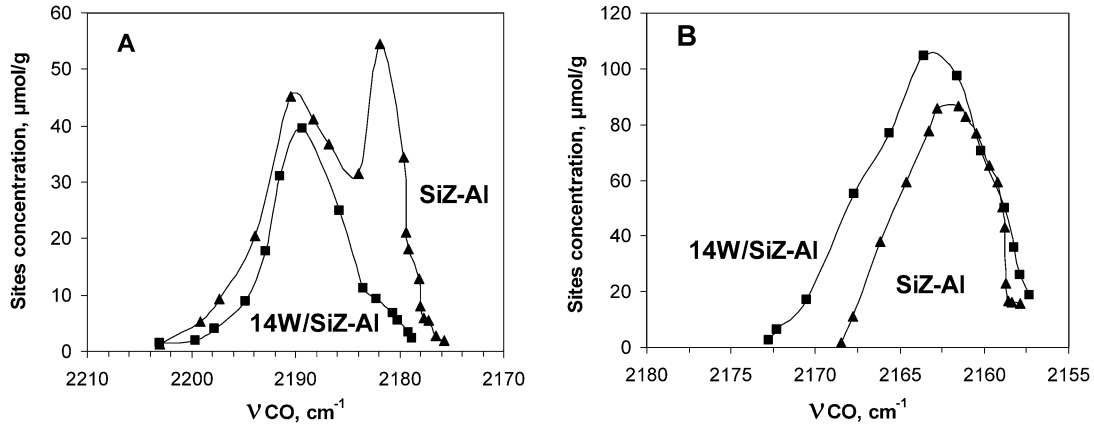

Fig. 12. Distributions of Lewis (A) and Brønsted (B) acid sites on the 14W/SiZ-Al and on the bare SiZ-Al extrudate samples.

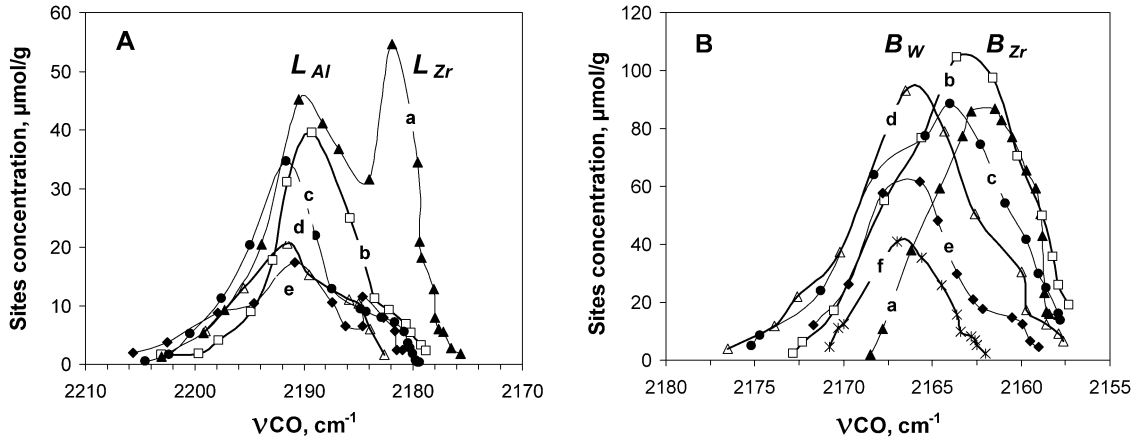

Fig. 13. Distributions of Lewis (A) and Brønsted (B) acid sites on the xW/SiZ-Al and on the bare SiZ-Al extrudate samples. (a) SiZ-Al, (b) 14W/SiZ-Al, (c) 16W/SiZ-Al, (d) 22W/SiZ-Al, (e) 27W/SiZ-Al, (f) 34W/SiZ-Al.

the monolayer is reached. Further loading does not affect the strength of the Brønsted sites, but their concentration strongly diminishes as the bulk WO_3 grows. Again, fitting the distributions strongly suggests that the shift in wave number results from the relative contributions of two kinds of Brønsted sites and not from a modification of the original zirconia sites.

In conclusion, drawing the acid distributions makes it possible to clarify and better interpret the complex spectra of these materials. This method reveals the bands characteristic of the interaction of CO with the surface: 2182 and 2162 cm^{-1} for the Lewis and Brønsted sites of the uncovered zirconia; 2191 cm^{-1} for the Lewis sites of the binder; and 2167 cm^{-1} for the new Brønsted acidity generated by tungstate. Note that this acidity remains moderate [34].

3.4.2. Acid site quantification: influence of tungsten loading

In principle, fitting the distributions with the bands attributed to the various acid sites should make it possible to quantify each species and determine how their concentration changes with the tungsten loading. However, some additional bands are present on the spectra of samples saturated with CO, and they were not taken into account in the distributions (i.e., interaction of CO with the silanol groups at 2156 cm^{-1} and physisorption at 2143 and 2131 cm^{-1}. Therefore, for a more accurate quantification, we deconvoluted the spectra with the contribution of seven bands, namely Lewis sites of alumina (L_{Al}, 2191 cm^{-1}) and of zirconia (L_{Zr}, 2182 cm^{-1}), Brønsted sites associated with tungsten (B_W, 2167 cm^{-1}) and zirconia (B_{Zr}, 2162 cm^{-1}), silanols (SiOH, 2156 cm^{-1}), and physisorption (Φ_1, 2143 cm^{-1} and Φ_2, 2131 cm^{-1}), assuming gaussian distributions. An example of deconvolution (14W/SiZ-Al catalyst) is given in Fig. 14.

The fit with the experimental spectrum is satisfactory. The same procedure was repeated for every sample of the xW/SiZ-Al series, keeping the same position and width for the various bands. Conversion of the areas into concentrations of sites was done with the same extinction coefficients of the Lewis and Brønsted CO bands for zirconia and tungstated zirconia samples. Results of the Lewis and Brønsted site concentrations on the xW/SiZ-Al extrudates are plotted in Fig. 15 versus tungsten loading.

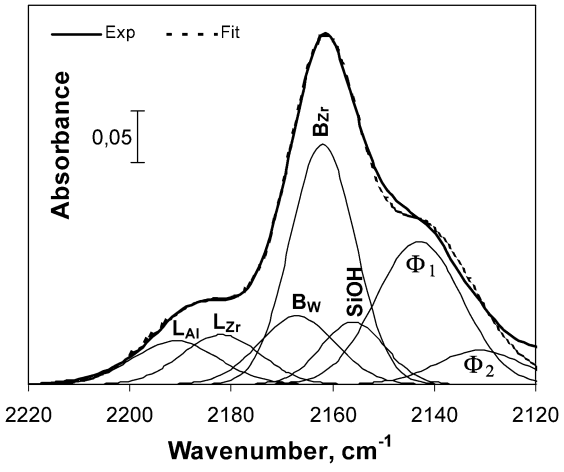

Fig. 14. Gaussian deconvolution of the IR spectrum of CO adsorbed at saturation on the 14W/SiZ-Al extrudate sample. See text for the legend.

The evolution of acid site concentration shows a singularity for every type of acidity at 22 wt% W, that is, at the monolayer coverage. Both the Lewis L_{Zr} and the Brønsted B_{Zr} acid sites of the zirconia carrier decrease linearly up to $\sim$6 W atoms nm^{-2} ZrO_2; their concentration becomes zero or very small beyond this point. The Lewis sites (L_{Al}) of the alumina binder are also informative since their concentration stays constant at first, then decreases at high tungsten loading, as bulk WO_3 is observed. Most interesting is the change in concentration of the strong Brønsted (B_W) sites associated with the tungsten species, with a maximum at the monolayer coverage. The concentration at the maximum amounts to $\sim$300 µmol g^{-1}, that is, $\sim$0.3 sites per tungsten atom. The curve shows a threshold for coverage at about half the monolayer, indicating that the first tungsten species do not induce protonic acidity. The slow decrease in the concentra-

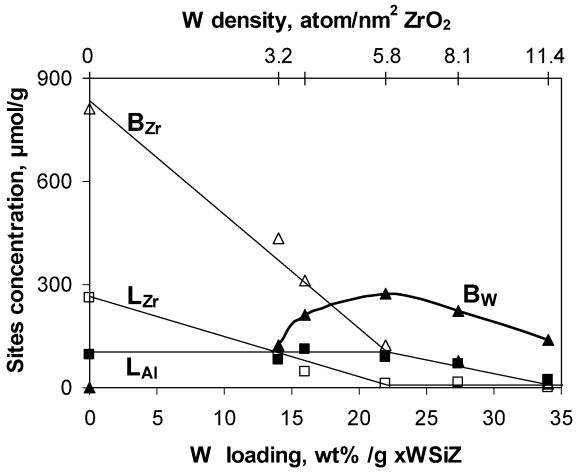

Fig. 15. Evolution of the various Lewis and Brønsted acid sites as a function of tungsten loading and tungsten density of the xW/SiZ-Al extrudates.

tion in B_W sites beyond the maximum corresponds again to the formation of bulk tungsten oxide. Thus, Brønsted acidity is created by tungstate at the expense of both Brønsted and Lewis zirconia sites, provided the polytungstate species do not segregate into bulk tungsten oxide.

3.4.3. Relation with the nature of tungsten species

The variations in the acid site concentrations should reflect the buildup of the tungstated zirconia catalyst, that is, the changes in nature of the supported tungsten species. The consumption of the Lewis sites of the zirconia is well accepted in the literature, attesting to the interaction of tungstate species with the carrier.

Recently it has been shown that tungsten forms a two-dimensional WO_x overlayer made up of oligomeric islands, growing with increasing tungsten concentration [3,11,13], and ultimately segregating into three-dimensional clusters beyond the monolayer coverage. In these studies, the classical distinction between monomeric and polymeric species with increasing tungsten concentration was not indicated. In contrast, the IR and Raman works by Kim et al. [19] and Gutierrez-Alejandre et al. [41] on a low loaded WZ sample pointed to isolated monooxo tungsten species and to the absence of W–O–W stretching modes assigned to polytungstate species, while they appear and develop at higher tungsten content [19]. However, the solids were not prepared in the same way: the former authors impregnated a structurally stable zirconia, and the latter carried out crystallization of zirconia in the presence of tungsten. This may influence the grafting of the first tungsten species. In any case, low loaded samples do not exhibit acidity. The domain of interest starts at about half the monolayer, where the new Brønsted sites develop.

According to Barton et al. [13], polytungstate domains grow by condensation of WO_x species. These domains of intermediate size may be slightly reduced, and charge compensation creates Brønsted acidity. The decrease in UV–visible absorption edge energy indicative of the growth of the domains coincides with an increase in the rate of several reactions. Although quite convincing, this interpretation does not fully explain our results. First, the authors find a maximum activity significantly beyond the monolayer coverage (~ 10 W nm^{-2}), where the polytungstate coexists with crystalline WO_3. The concentration of stronger sites that we identified on our samples by CO at 2167 cm^{-1} is at maximum at the monolayer (~ 6 W nm^{-2}) and, as shown in the next paper, correlates very well with the isomerization activity. Similar results on Brønsted acidity, correlated with skeletal isomerization, were also observed by Naito et al. [15], who used improved ammonia TPD and IR spectroscopy of pyridine adsorption. Second, the results of acid titration reported for the WZ [13] samples did not permit the correlation of acidity with activity in the whole range of tungsten densities, especially at high coverage. The number of Brønsted sites at maximum is very low, 0.04 H^+ per W atom [23] or even lower [24], for bases as titrants, and 0.063 H^+/W from hydrogen uptake [14]. Therefore, according to Baertsch et al. [23], the stabilization of one H^+ site requires an ensemble of ~ 25 W atoms. These values are very far from that obtained in our study with carbon monoxide and that reported by Naito et al. [15]. The site density amounts to as much as ~ 0.3 H^+/W at the monolayer. Apparently, the active phase of our samples accommodates one site for about three W atoms, a value similar to that for Keggin clusters. Scheithauer et al. [11] already proposed a surface pseudo-heteropolyanion structure with charge-compensating protons. The authors provided spectroscopic identification of W–O–W linkages and W=O terminal groups and determined an increase from two to five in the number of nearest W neighbors. They postulated a WO_x network in a two- to three-dimensional growing overlayer as the loading reaches the saturation of the zirconia surface. The negative charge of the W=O octahedral environment in the structurally poorly defined tungstate overlayer is compensated for by a proton. Incorporation of Zr^{4+} ions would also require charge compensation in a pseudo-heteropolyanion. This structure generates the Brønsted acidity as a permanent property of the solids rather than transient protons formed in the presence of hydrogen. Unfortunately, the authors did not quantify the amount of sites, using the infrared signal of adsorbed carbon monoxide. In our present study, we could resolve the band shift of the interaction of CO with Brønsted acidity. The strong acid sites that we identified on our samples by CO at 2167 cm^{-1} are associated with (poly)tungstate and will be seen to correlate with the isomerization activity. Although the catalysts contain platinum and have been activated under hydrogen, we believe that our samples do not require hydrogen to exhibit acidity because they have been evacuated before titration measurements with carbon monoxide. It cannot be excluded that in the reduction step of the catalysts, tungsten is reduced to some extent, as has been shown recently [42]. Consequently, H^+ would be incorporated into the polyoxo cluster and act as acidic protons, but with lower acid strength than those already present. How-

ever, the stoichiometry of one site for three W atoms is fairly in line with the heteropolyanion structure proposed by Scheithauer et al. [11]. This leads us to favor this latter hypothesis. It is difficult to understand the large difference in site density with that reported by the group of Iglesia. We speculate that in the course of the preparation of the samples the prolonged contact of tungsten precursor with hydrous zirconia favors the incorporation of Zr^{4+} ions into the polytungstate structure. This would not occur or would occur to a much lesser extent during impregnation by incipient wetness.

The proposal of heteropolyanion can be adapted in our case by substituting Si^{4+} for Zr^{4+}. This hypothesis could explain the broad structural band around 1100 cm^{-1} (Fig. 10A), which should be attributed to Si–O vibrations in a Keggin-like structure. Indeed, SiOH groups are readily consumed when silica-stabilized zirconia is loaded with tungsten. It has been reported that silica containing tungsten heteropolyanion is formed easily upon impregnation of silica with tungstate [43]. However, in the case of a silica carrier, these structures are partially decomposed upon calcination above 673 K. In our case, the structure is most probably stabilized by grafting to the zirconia surface.

To summarize, a detailed analysis of the IR spectra of adsorbed CO at low temperature has distinguished different Lewis and Brønsted acid sites on alumina extrudates of tungstated zirconia. The effect of tungsten loading has shown that the tungstate species are grafted on the zirconia surface. They consume both Lewis and Brønsted acid sites of the zirconia up to the monolayer. A new moderate Brønsted acidity, created in the polytungstate domain, has been detected by CO at about 2167 cm^{-1}. The concentration of these acid sites amounts to one site for about three tungsten atoms at the monolayer. Beyond the monolayer, the acidity decreases because of the formation of WO_3 bulk oxide from the polytungstate species.

3.5. Metallic function: accessibility of platinum from hydrogenation of toluene and CO adsorption

The yPt/xW/SiZ-Al samples will be used as catalysts in the skeletal isomerization of *n*-hexane. It is therefore important to characterize the platinum component of the catalysts. This was done by means of toluene hydrogenation and carbon monoxide adsorption. The combined measurements proved to be very informative in the case of platinum supported on sulfated zirconia [9]. In the same work, we showed that platinum located on the alumina binder (if any) plays a negligible role in the catalysis. Indeed, we demonstrated that the platinum accessibility was limited at low loading because a fraction of the metal was incorporated into the zirconia matrix. We applied that method to determine the number of exposed platinum atoms supported on the tungstated zirconia samples examined in this study. We also verified that platinum did not influence the acid property of the solids.

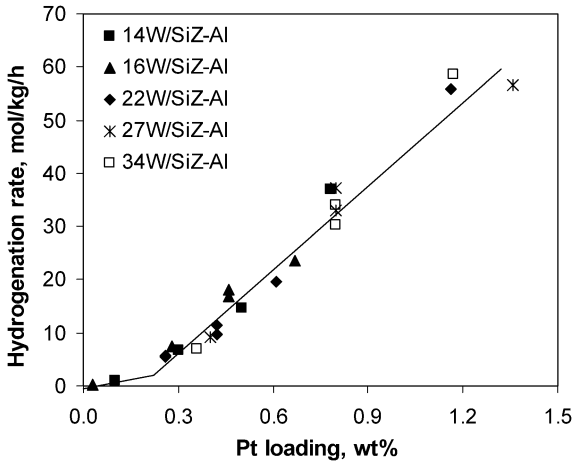

Fig. 16. Toluene hydrogenation rates at 423 K as a function of platinum loading on the yPt/xW/SiZ-Al catalysts.

3.5.1. Hydrogenation of toluene

Hydrogenation of toluene at atmospheric pressure was measured at 423 and 523 K on the yPt/xW/SiZ-Al catalysts reduced at 523 K. At 423 K and at low conversion, the reaction was totally selective in hydrogenation into methylcyclohexane. Isomerization products, such as dimethylcyclopentanes, were detected at 523 K, indicating that the acidic function of the catalysts was active at this temperature. Ring opening by hydrogenolysis on the metal did not occur under our experimental conditions.

The hydrogenation rates measured at 423 K on the series of yPt/xW/SiZ-Al catalysts containing increasing amounts of platinum are plotted in Fig. 16. The plot is similar to that observed for platinum supported on sulfated zirconia [9]. Two linear domains are clearly distinguished. Catalysts with a low Pt loading (below 0.2 wt% Pt) have a poor activity, whereas hydrogenation develops in the second domain, beyond ca. 0.2 wt% Pt. Increasing the reaction temperature to 523 K does not change the observation. The proportionality of activity with Pt loading within each domain points to a constant dispersion of platinum. Moreover, since all of the samples are represented on the same lines of the plot, this dispersion is unaffected by the tungsten loading, below or beyond the monolayer.

3.5.2. FT-IR of adsorbed carbon monoxide: determination of accessible platinum

CO adsorption at room temperature monitored by infrared spectroscopy was used to measure the platinum dispersion on the tungstated zirconia-based catalysts. At this temperature, CO does not interact with the acid sites. Typical spectra for incremental adsorbed doses of CO are displayed in Fig. 17 for the 14W/SiZ-Al sample containing 0.3 wt% platinum.

CO adsorption at room temperature indicates that platinum is in the metallic state; the band at 2079 cm^{-1} is characteristic of the linear adsorbed species. Bridged species are also observed at 1858 cm^{-1} for CO doses exceeding

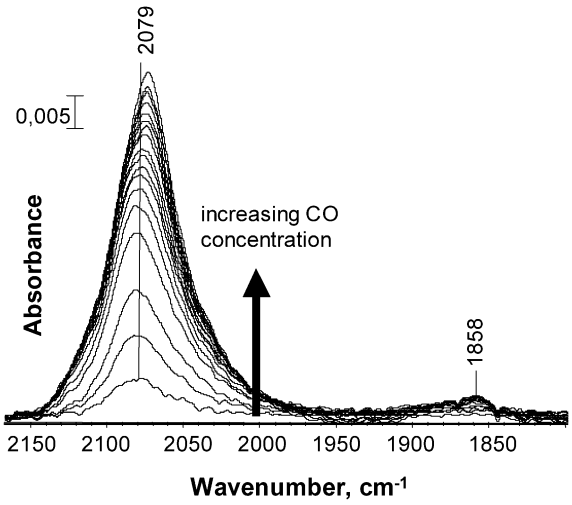

Fig. 17. FT-IR spectra of adsorbed CO at room temperature on the 0.3Pt/14W/SiZ-Al catalyst. CO concentration was increased from 0.4 to 50 µmol CO g^{-1}.

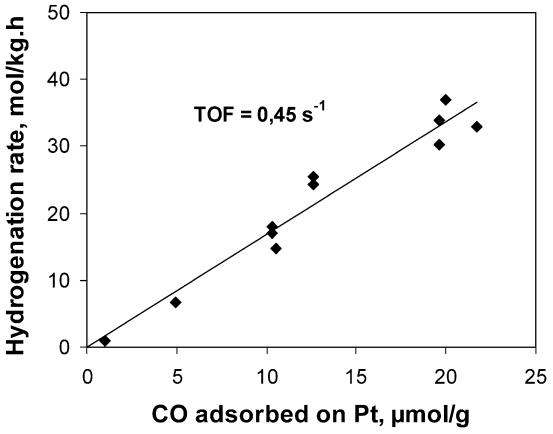

Fig. 18. Relation between the amount of CO adsorbed at saturation and the hydrogenation rate measured at 423 K for the series of yPt/xW/SiZ-Al catalysts.

saturation. Simultaneously, the band shifts slightly to lower wave number because of lateral interactions of adsorbed CO. Similar features of platinum are recorded for every catalyst, independently of the tungsten content. Each data point gives access to the number of accessible platinum adsorption sites at saturation of the surface, with the use of the breakpoint method of Binet et al. [44] in the plot of the area of the IR signal versus CO concentration.

Finally, combining, for the whole series of yPt/xW/SiZ-Al catalysts, the titration of surface platinum by CO with the activity in hydrogenation of toluene yields the good linear correlation in Fig. 18. This is in perfect agreement with the previous characterization of platinum on sulfated zirconia catalysts [9]. It confirms that the poorly hydrogenating properties of the low loaded catalysts are due to a lack of accessible platinum, most probably because Pt species have been trapped in the zirconia subsurface.

The amount of imbedded Pt reaches a limit when the zirconia subsurface is saturated. It can be calculated from the two branches in the hydrogenation plot (Fig. 16). On the yPt/xW/SiZ-Al samples, as much as 89% of total platinum is trapped at low loading, and saturation occurs at 0.23 wt% Pt. It is significantly higher than on the previous sulfated zirconia samples (0.15 wt% Pt at saturation [9]), which is probably due to a different preparation. Since the hydrogenation rate is proportional to accessible platinum, the low loaded catalysts are much less active than the samples belonging to the second domain, after saturation. However, the turnover frequency, 0.45 s^{-1}, is similar. Correcting the total platinum content from the inactive subsurface species makes it possible to determine the real dispersion and the particle size of the external platinum crystallites from CO adsorption. For all of the samples studied, we found a constant particle size of about 1.2 nm, corresponding to 70% real dispersion of external platinum. This agrees with the value obtained on sulfated zirconia. As already stated [9], the occurrence of such "buried" platinum species offers a rational interpretation of the low hydrogen chemisorption capacity at low platinum loading and the unusual values for the metal dispersion reported in the literature [38,45,46].

To conclude, our yPt/xW/SiZ-Al samples exhibit well-dispersed accessible metallic platinum. The excellent correlation between CO chemisorption and hydrogenation of toluene makes it possible to determine the concentration of surface sites by the simple catalytic test. These results will be related in Part II to catalytic activity for *n*-hexane isomerization.

4. Conclusions

Platinum tungstated zirconia isomerization catalysts were characterized by XRD, nitrogen adsorption–desorption, and infrared spectroscopy of adsorbed CO. A silica-doped hydrous zirconia was used to prepare the tungstated zirconia samples containing 14–34 wt% W, which were extrudated with an alumina binder. It is shown that after calcination at 1023 K, silica stabilizes the crystalline zirconia in the tetragonal phase and yields high surface area and porosity. The structural and textural properties of the silica-stabilized zirconia are not influenced by tungsten. Bulk WO_3 tungsten oxide is detected for tungsten loading exceeding the monolayer at ∼6 atoms W nm^{-2} ZrO_2 and provokes the rupture of the physical binding of alumina. Low-temperature FT-IR spectra of adsorbed carbon monoxide revealed four types of acidity: Lewis sites on zirconia and on alumina, and Brønsted sites on zirconia and on tungstate species. Their distribution varied with tungsten loading. Both Lewis and Brønsted acid sites of zirconia are consumed up to the monolayer coverage, whereas the acid sites of alumina are hardly affected. A new moderate Brønsted acidity associated with polytungstate species ($\nu_{CO} = 2167$ cm^{-1}, stronger than that on zirconia) is created at intermediate tungsten cov-

erage. The concentration of these Brønsted sites increases with tungsten loading and reaches a maximum of one H^+ for about three tungsten atoms at the monolayer. Beyond, this acidity diminishes because of the formation of bulk tungsten oxide at the expense of polytungstate species. The high density of sites is tentatively interpreted by the formation of a pseudo-heteropolyanion incorporating Zr^{4+} ions and most likely Si^{4+} ions, in line with the new infrared signal at about 1250–1050 cm^{-1} in the structure band region.

The platinum component (0.1–1.5 wt%) was investigated by CO adsorption at room temperature and hydrogenation of toluene. The accessible platinum detected by infrared spectroscopy of CO adsorption is in the metallic state. A good relation between the two methods was observed. Two linear domains were detected with increasing platinum content, with a sharp increase at about 0.23 wt% Pt. It is suggested that at low content, most of the metal is inserted into the zirconia matrix, resulting in a lack of accessible metal. After the saturation of the subsurface, additional platinum remains on the external surface and thus is accessible. A high dispersion (about 70%) with a constant particle size of about 1.2 nm for accessible platinum is found in the whole range of platinum concentration.

This in-depth characterization of the acidic and metallic functions of such bifunctional catalysts will be used in the second part of this article to help rationalize the hydroisomerization results for *n*-hexane.

Acknowledgments

T.N.V. gratefully acknowledges Total for financial support. We thank Y.L. Tea for the sample preparation and M.C. Basset and J. Quillard for their help with BET and catalytic measurements.

References

[1] M. Hino, K. Arata, J. Chem. Soc. Chem. Commun. (1980) 851.
[2] M. Hino, K. Arata, J. Chem. Soc. Chem. Commun. (1987) 1259.
[3] E. Iglesia, D.G. Barton, S.L. Soled, S. Miseo, J.E. Baumgartner, W.E. Gates, G.A. Fuentes, G.D. Meitzner, Stud. Surf. Sci. Catal. 101 (1996) 533.
[4] D.G. Barton, S.L. Soled, E. Iglesia, Top. Catal. 6 (1998) 87.
[5] S. Kuba, P. Lukinskas, R.K. Grasselli, B.C. Gates, H. Knözinger, J. Catal. 216 (2003) 553.
[6] S. Kuba, P. Lukinskas, R. Ahmad, F.C. Jentoft, R.K. Grasselli, B.C. Gates, H. Knözinger, J. Catal. 219 (2003) 376.
[7] F.T.T. Ng, N. Horvat, Appl. Catal. A 123 (1995) L197.
[8] K.B. Fogash, Z. Hong, J.M. Kobe, J.A. Dumesic, Appl. Catal. A 172 (1998) 107.
[9] J. van Gestel, T.N. Vu, D. Guillaume, J.P. Gilson, J.C. Duchet, J. Catal. 212 (2002) 173.
[10] K. Arata, M. Hino, M.J. Phillips, M. Ternan (Eds.) in: Proceedings of the 9th International Congress on Catalysis, Calgary, vol. 4, 1988, p. 1727.
[11] M. Scheithauer, R.K. Grasselli, H. Knözinger, Langmuir 14 (1998) 3019.
[12] M. Scheithauer, T.K. Cheung, R.E. Jentoft, R.K. Grasselli, B.C. Gates, H. Knözinger, J. Catal. 180 (1998) 1.
[13] D.G. Barton, S.L. Soled, G.D. Meitzner, G.A. Fuentes, E. Iglesia, J. Catal. 181 (1999) 57.
[14] C.D. Baertsch, S.L. Soled, E. Iglesia, J. Phys. Chem. B 105 (2001) 1320.
[15] N. Naito, N. Katada, M. Niwa, J. Phys. Chem. B 103 (1999) 7206.
[16] K. Shimizu, T.N. Venkatraman, W. Song, Appl. Catal. A 225 (2002) 33.
[17] G. Ferraris, S. De Rossi, D. Gazzoli, I. Pettiti, M. Valigi, G. Magnacca, C. Morterra, Appl. Catal. A 240 (2003) 119.
[18] S.R. Vaudagna, S.A. Canavese, R.A. Comelli, N.S. Figoli, Appl. Catal. A 168 (1998) 93.
[19] D.S. Kim, M. Ostromecki, I.E. Wachs, J. Mol. Catal. A 106 (1996) 93.
[20] R.A. Boyse, E.I. Ko, J. Catal. 171 (1997) 191.
[21] G. Busca, J. Raman Spectrosc. 33 (2002) 348.
[22] D.G. Barton, M. Shtein, R.D. Wilson, S.L. Soled, E. Iglesia, J. Phys. Chem. B 103 (1999) 630.
[23] C.D. Baertsch, K.T. Komala, Y.H. Chua, E. Iglesia, J. Catal. 205 (2002) 44.
[24] J.G. Santiesteban, J.C. Vartuli, S. Han, R.D. Bastian, C.D. Chang, J. Catal. 168 (1997) 431.
[25] P. Da Silva, M. Bisson, A. Millan, French Patent 2,793,706 (1999).
[26] C. Morterra, G. Cerrato, V. Bolis, C. Lamberti, L. Ferroni, L. Montanaro, J. Chem. Soc. Faraday Trans. 91 (1) (1995) 113.
[27] C. Morterra, G. Cerrato, L. Ferroni, Mater. Chem. Phys. 37 (1994) 243.
[28] J.C. Duchet, D. Guillaume, A. Monnier, C. Dujardin, J.P. Gilson, J. van Gestel, G. Szabo, P. Nascimento, J. Catal. 198 (2001) 328.
[29] D.J. Zalewski, S. Alerasool, P.K. Doolin, Catal. Today 53 (1999) 419.
[30] R. Olindo, F. Pinna, G. Strukul, P. Canton, P. Riello, G. Cerrato, G. Meligrana, C. Morterra, Stud. Surf. Sci. Catal. 130 (2000) 2375.
[31] T. Lei, J.S. Xu, W.M. Hua, Y. Tang, Z. Gao, Catal. Lett. 61 (1999) 213.
[32] C. Morterra, G. Cerrato, S. Di Ciero, Appl. Surf. Sci. 126 (1998) 107.
[33] C. Morterra, G. Cerrato, F. Pinna, Spectrochim. Acta, Part A 55 (1999) 95.
[34] O. Cairon, T. Chevreau, J.C. Lavalley, J. Chem. Soc. Faraday Trans. 94 (1998) 3039.
[35] A. Zecchina, E. Escalona Platero, C. Otero Arean, J. Catal. 107 (1987) 244.
[36] A. Travert, O.V. Manoilova, A.A. Tsyganenko, F. Maugé, J.C. Lavalley, J. Phys. Chem. B 106 (2002) 1350.
[37] M. Valigi, D. Gazzoli, I. Pettiti, G. Mattei, S. Colonna, S. De Rossi, G. Ferraris, Appl. Catal. A 231 (2002) 159.
[38] J.M. Grau, J.C. Yori, J.M. Parera, Appl. Catal. A 213 (2001) 247.
[39] A. Punnoose, M.S. Seehra, I. Wender, Fuel Process. Technol. 74 (2001) 33.
[40] L.M. Petkovic, J.R. Bielenberg, G. Larsen, J. Catal. 178 (1998) 533.
[41] A. Gutierrez-Alejandre, P. Castillo, J. Ramirez, G. Ramis, G. Busca, Appl. Catal. A 216 (2001) 181.
[42] S. Kuba, M. Che, R.K. Grasselli, H. Knözinger, J. Phys. Chem. B 107 (2003) 3459.
[43] X. Xia, R. Jin, Y. He, J.F. Deng, H. Li, Appl. Surf. Sci. 165 (2000) 255.
[44] C. Binet, A. Jadi, J.C. Lavalley, J. Chim. Phys. 86 (1989) 451.
[45] M.G. Falco, S.A. Canavese, R.A. Comelli, N.S. Figoli, Appl. Catal. A 201 (2000) 37.
[46] J.C. Yori, J.M. Parera, Catal. Lett. 65 (2000) 205.